The Cryosphere Discuss., 3, 919–946, 2009
www.the-cryosphere-discuss.net/3/919/2009/

The Cryosphere Discussions

This discussion paper is/has been under review for the journal The Cryosphere (TC).
Please refer to the corresponding final paper in TC if available.

Multi-channel ground-penetrating radar to explore spatial variations in thaw depth and moisture content in the active layer of a permafrost site

U. Wollschläger[1], **H. Gerhards**[1], **Q. Yu**[2], **and K. Roth**[1]

[1]Institute of Environmental Physics, Heidelberg University, 69120 Heidelberg, Germany
[2]State Key Laboratory of Frozen Soil Engineering Cold and Arid Regions Environmental and Engineering Research Institute, CAS, Lanzhou, China

Received: 9 October 2009 – Accepted: 14 October 2009 – Published: 2 November 2009

Correspondence to: U. Wollschläger (ute.wollschlaeger@iup.uni-heidelberg.de)

Published by Copernicus Publications on behalf of the European Geosciences Union.

Abstract

Multi-channel ground-penetrating radar was applied at a permafrost site on the Tibetan Plateau to investigate the influence of surface properties and soil texture on the late-summer thaw depth and average soil moisture content of the active layer. Measurements were conducted on an approximately 85×60 m^2 sized area with surface and soil textural properties that ranged from medium to coarse textured bare soil to finer textured, vegetated areas covered with fine, wind blown sand, and it included the bed of a gravel road. The survey allowed a clear differentiation of the various units. It showed (i) a shallow thaw depth and low average soil moisture content below the sand-covered, vegetated area, (ii) an intermediate thaw depth and high average soil moisture content along the gravel road, and (iii) an intermediate to deep thaw depth and low to intermediate average soil moisture content in the bare soil terrain. From our measurements, we found plausible hypotheses for the permafrost processes at this site leading to the observed late-summer thaw depth and soil moisture conditions. The study clearly indicates the complicated interactions between surface and subsurface state variables and processes in this environment. In addition, the survey demonstrates the potential of multi-channel ground-penetrating radar to efficiently map thaw depth and soil moisture content of the active layer with high spatial resolution at scales from a few meters to a few kilometers.

1 Introduction

Permafrost on the Tibetan Plateau reacts very sensitively to climate change (Liu and Chen, 2000). This is manifest in a rise in the lower limit of the altitudinal permafrost, increase in active layer thickness and ground temperature, intensification in freeze-thaw cyles and heat exchange between soil and atmosphere, and lowering of ground water and lake water levels with related desertification caused by the drier ground surface (Cheng and Wu, 2007).

In cold regions, the active layer is "the layer of ground that is subject to annual thawing and freezing in areas underlain by permafrost" (van Everdingen, 1998). In this environment, it plays a significant role since almost all biogeochemical, hydrological, ecological, and pedogenic processes take place in this uppermost part of the soil (Kane et al., 1991; Hinzman et al., 2005). The thaw depth of the active layer determines, for instance, the partitioning of surface and groundwater runoff, it influences the rate of water and gas exchange between the soil and the atmosphere (Duguay et al., 2005) and the occurence of specific vegetation communities (Kane et al., 1991; Walker et al., 2003), and it also has a significant importance for cold regions engineering (Nelson et al., 2001).

From a large-scale perspective, the thaw depth of the active layer primarily depends on temperature and the length of the thaw season (Hinzman et al., 2005). The seasonal thaw depth, however, is locally influenced by various additional factors that affect the local microclimate and surface energy balance. Important factors are surface temperature, physical and thermal properties of the surface cover and the substrate, vegetation cover, soil moisture content, albedo, and thickness and duration of snow cover (Duguay et al., 2005; Hinzman et al., 2005).

Monitoring of active layer freeze and thaw processes is most often based on point measurements like boreholes (e.g. Brown et al., 2000; Liu and Chen, 2000). However, at point locations, year-to-year and microtopographic variations in surface temperature and soil moisture content can induce large spatial variations in thaw depth (Lemke et al., 2007) which leads to difficulties for interpreting larger-scale active layer dynamics using borehole data, e.g. if detailed processes being relevant at the ecosystem scale should be addressed. Examples for active layer thaw depth variability are given, e.g. by Wright et al. (2009) for small-scale variations and by Hinkel and Nelson (2003) for larger areas. Hence, in order to obtain a deeper understanding of active layer processes, efficient methods which allow mapping of active layer conditions such as thaw depth and soil moisture content are desired.

In order to derive large-scale spatial information about permafrost conditions, vari-

ous satellite remote sensing techniques are currently being applied (Zhang et al., 2004; Duguay et al., 2005). So far, the challenge with mapping near-surface permafrost conditions from space is that only information about surface properties is available. Subsurface phenomena then have to be deduced from these data (Duguay et al., 2005). However, due to the various surface and subsurface factors and processes influencing the thaw process, estimation of active layer thaw depth from remote sensing measurements is still challenging (Zhang et al., 2004; Duguay et al., 2005).

At an intermediate scale, ranging from a few meters to a few kilometers, ground-based geophysical measurements yield spatially highly resolved information on soil material properties and state variables like soil moisture content. This opens a way for a more detailed investigation of processes relevant at the ecosystem scale. In permafrost regions, ground-penetrating radar (GPR) has been proven to be well suited for studying near-surface phenomena which are related to soil moisture and ice content, respectively. Starting with the pioneering work of Annan and Davis (1976) GPR by now has been applied in various permafrost studies, e.g. for mapping the depth of the permafrost table (Arcone et al., 1998; Hinkel et al., 2001; Moorman et al., 2003; Schwamborn et al., 2008) or layer boundaries in frozen ground (Hinkel et al., 2001), exploring massive ground ice (Annan and Davis, 1976) and pingo ice (Yoshikawa et al., 2006), ice wedges (Hinkel et al., 2001; Munroe et al., 2007), or thaw depth beneath streams (Bradford et al., 2005; Brosten et al., 2006, 2009). In addition, GPR has been employed to infer the near-surface moisture content of the active layer from the analysis of ground wave measurements (Moorman et al., 2003).

The measurement principle of GPR is based primarily on the analysis of the propagation velocity of electromagnetic waves travelling through the ground. The propagation velocity predominantly depends on the soil's dielectric permittivity which itself is directly related to the water and ice content, respectively (Davis and Annan, 1989). Reflections occur at interfaces that are related to abrupt changes in dielectric permittivity, e.g. at layer boundaries, at a groundwater table in a coarse-textured soil or at the frozen-unfrozen ground interface. Hence, in permafrost studies, GPR can be em-

ployed to spatially distinguish between wet and dry areas as well as between frozen an unfrozen sections within the soil. Due to the strong dielectric contrast between the frozen and the overlying unfrozen active layer, the frost table usually appears as a well detectable, continuous reflector in the radargram.

The major drawback of the typical common offset, single channel GPR measurements is, that the travel time measured to estimate the depth of a reflector strongly depends on the dielectric permittiviy of the ground as well. Hence, there are two unknown quantities, typically variable both in space and time, that determine the single measurement quantity. A common work-around is to calibrate dielectric permittivity and the related reflector depths with additional measurements, e.g. in boreholes (e.g. Arcone et al., 1998; Lunt et al., 2005), at excavates of soil profiles (e.g. Wollschläger and Roth, 2005) or common-midpoint (CMP) GPR measurements (e.g. Schwamborn et al., 2008). All this is practically feasible at only a few locations. However, due to the heterogeneous texture of natural soils, soil moisture content and consequently dielectric permittivity typically vary horizontally over rather short distances (e.g. Greaves et al., 1996). This results in distortions of reflector depth as displayed in a radargram if a constant signal propagation velocity for the complete transect is assumed (Neal, 2004). Hence, estimates of reflector depth which are calibrated at only a few points along the measurement transect are only able to provide a rough estimate of the true reflector structure.

An efficient way to obtain more accurate information about the true shape of the reflector and additionally infer average soil moisture content are continuous multi-offset measurements obtained from multi-channel GPR systems (Bradford, 2008; Gerhards et al., 2008). Here, the survey is done in the profiling mode with an array of several coupled GPR antennas which allows to measure the travel times from a number of different antenna separations at once. The acquired data can then be evaluated in analogy to a standard CMP survey while the distance between the CMP data sets is determined by the pre-selected trace interval (e.g. each 0.1 m). Given suitable, continuous reflectors, this new measurement technique allows to infer high-resolution spatial information

about the reflector structure and average soil moisture content without requiring much additional data for calibration.

The objective of our study is to apply multi-channel GPR at a continuous permafrost site in order to efficiently infer spatial variations in thaw depth and average volumetric soil moisture content of the active layer. In the following, the expression "soil moisture content" refers to the liquid volumetric water content which is measurable with the GPR technique. In order to demonstrate the applicability of multi-channel GPR to investigate permafrost processes at the ecosystem scale, the observed patterns are interpreted with respect to the found surface and soil properties.

2 Site description

The study site is located near the Qitedaban mountain pass (35° 45′ N, 79° 26′ E, 4950 m a.s.l.), in the northern Aksai Chin Region, Xinjiang Province, W-China (Fig. 1). This western part of the Qinghai-Tibet Plateau is mainly characterised by high-cold desert landscapes (Jin et al., 2007). Being situated in the rain shadow of the Karakorum and Kunlun mountain ranges, annual convective precipitation in the area is less than 50 mm which is occasionally enhanced by monsoon rainfall (Gasse et al., 1991). The ratio of evaporation to precipitation ranges between 20 and 50 (Gasse et al., 1991) indicating the extremely arid climate of the study area. The present-day permafrost limit in the W-Kunlun region is located between 4400 m and 4500 m a.s.l. (Zhou et al., 1998). According to the chinese classification, the site is situated within an area of extensive dicontinuous permafrost (Zhou and Guo, 1983; Zhou et al., 2000).

Measurements were conducted at the foot of an alluvial fan (Fig. 2). The soil surface at the upper part of the slope is almost bare. It is covered with a number of small flow channels which were dry during the survey. During an earlier measurement campaign in summer 2006 (Gerhards et al., 2008) some of the channels were water bearing but surface water infiltrated completely before reaching the foot of the slope. In a soil profile which was excavated a few hundred meters upslope of the measurement plot a

groundwater table was observed at a depth of 0.76 m below the ground surface. The soil of the alluvial fan primarily consists of sand and gravel. Several finer textured areas can be identified by salt precipitations appearing at the soil surface. They indicate the higher water retention capacity of the fine grained soil which makes the soil water available for evaporation close to the ground surface. At the foot of the alluvial fan, on both sides of the Xinjiang-Tibet Highway, small vegetated areas occur. In the valley bottom, a dry river bed extends parallel to the gravel road. In some sections it is located upslope of the gravel road, then crosses the highway and continues in the downslope area of the road.

In order to spatially investigate the influence of surface properties and soil texture on the thaw depth and average soil moisture content of the active layer, we selected an approximately 85×60 m^2 sized plot at the foot of the slope where the soil surface was partially bare and partially covered with sparse grass (Fig. 2). In addition, the area is traversed by the Xingjiang-Tibet Highway, which represents another textural unit of our study site. The soil beneath the bare surface basically consists of medium to coarse grained sand and gravel. Below the vegetated area the soil is characterised by rather homogeneous fine to medium grained sand which is covered by a 10 to 15 cm thick layer of even finer, presumably wind-blown sand that has been accumulated by the sparse grass cover. Within the vegetated area, precipitations of salt were observed on the soil surface. The surface salt indicates the high amount of evaporation from the fine textured soil in this area. The sand accumulations within the vegetated patch produce a rough, slightly elevated surface topography with a maximum height of about 0.5 m (Fig. 2).

3 Materials and methods

Multi-channel GPR measurements were acquired on 31 August 2007 when the annual thaw depth of the active layer was presumed to be close to its deepest position. The site was explored by measuring eight parallel lines (Fig. 2) starting upslope of the vegetated

area with one profile covering a complete transect of bare soil. The following three lines started and finished on bare soil while crossing the vegetated area in-between. The next profile was measured in the roadside ditch of the Xinjiang-Tibet Highway and was followed by a line located directly on the gravel road. Finally, two more transects on the opposite side of the highway were explored. Here, in the valley bottom, the soil surface was again partially covered by sparse vegetation.

Measurements were done with a multi-channel GPR array (Fig. 3a, b) that consisted of three standard 200 MHz shielded antenna systems (TR 200 K2) in combination with a DAD K2–MCH control unit and the distribution box (4CH), all manufactured by IDS (Ingegneria dei Sistemi S.p.A., Italy). The antenna boxes were coupled in a row with a fixed distance of 1.01 m between the two front antennas and a distance of 2.015 m separating both rear antennas. As in a standard common-offset survey the whole antenna array was pulled along the transect while signals were triggered by the survey wheel which was mounted to the back of the rear antenna.

The spatial position of the GPR array and surface topography were recorded using a TCRA1102 tachymeter (Leica GeoSystems, Germany). The survey lines were mapped by the tachymeter by automatically tracking a 360° reflector mounted on top of the middle antenna (Fig. 3a, b).

The multi-channel GPR system allows to acquire data from a total of nine transmitter–receiver combinations (Fig. 3b) while the multi-channel unit is capable to simultaneously record signals arriving from eight channels. For our survey we chose to measure radargrams with the following antenna separations: 2×0.19 m (T2–R2; T3–R3), 0.82 m (T2–R1), 1.2 m (T1–R2), 1.83 m (T3–R2), 2.21 m (T2–R3), 2.84 m (T3–R1), and 3.22 m (T1–R3). In order to be able to calculate reflector depth from the acquired measurements, data from the different channels have to be relocated such that the measurement position of each transmitter–receiver pair corresponds to the same location along the survey line. This provides several small CMP datasets (Fig. 3c) which, in case of good data quality, ideally consist of data recorded with seven different antenna separations (two of the eight available channels have the same an-

tenna separation). In this investigation, we used the position of the reflector of the laser tachymeter (Fig. 3b) as reference position for the relocation procedure. Since the survey is run in the normal profiling mode, the separation between the CMP data sets is equal to the spatial trace increment which was set to 0.05 m. By this moving CMP technique, we are able to efficiently estimate relative dielectric permittivity, reflector depth and average soil moisture content for each individual position along the radargram.

Radargrams were recorded using a time window of 100 ns, with a sampling rate of 10 samples per ns and 24 stacks per trace. Data processing was minimal and consisted of (i) shifting each radargram laterally to a common measurement position below the reflector of the tachymeter, (ii) application of a dewow filter in order to remove low frequency noise, (iii) clipping of all radargrams to a total travel time of 80 ns, and (iv) adjustment of the color density for each radargram individually for visualisation purposes. No amplification was applied on the data set. Next, the travel times of the frozen/unfrozen boundary reflection were picked in each radargram and air wave travel times were determined as a reference for the calculation of the absolute travel times of the reflected waves (Fig. 4).

Determination of relative dielectric permittivity, reflector depth and average soil moisture content of the active layer was done by applying the multi-channel evaluation procedure of Gerhards et al. (2008). Based on a ray approach, the method assumes that the two-way travel time t [ns] of the electromagnetic signal to a reflector at a position x [m] in the surroundings of the reference position x_0 [m] and antenna separation a [m] is given as

$$t(x;a) = \frac{\sqrt{\varepsilon_c}}{c_0}\cos(\alpha)\sqrt{4[d+[x_0-x]\tan(\alpha)]^2+a^2} \quad (1)$$

where ε_c [–] is the relative dielectric permittivity of the soil, c_0 is the speed of light in vaccuum (0.3 mns^{-1}), α is the reflector's inclination angle, and d [m] it's depth at x_0. Relative dielectric permittivity of the soil, depth and inclination angle of the reflector for every position along the radargram are estimated from the absolute travel times of the

signals measured with all available transmitter–receiver combinations. This is done by minimizing the objective function

$$OF(\mathbf{b}) = \sum_{(n,k)}^{(N,K)} \left(t_{\text{refl}}(x_n, a_k) - t_{\text{model}}(x_n, a_k; \mathbf{b}) \right)^2 \quad (2)$$

where $\mathbf{b}=\{\varepsilon_c, d, \alpha\}$ is the parameter vector, t_{refl} [ns] and t_{model} [ns] are the measured and modelled reflected wave travel times for N measurements around x_0 obtained from K antenna separations, x_n (n = 1, ..., N) are measurement points around x_0, and a_k (k = 1, ..., K) are the antenna separations. Since, due to low data quality, picking of reflections along certain sections of single radargrams sometimes is not possible, the evaluation program automatically conducts the inversion with all data which are available for the pre-defined distance interval around x_0 which was set to 0.5 m for this survey. With respect to the trace interval of 0.05 m and ideally data from eight channels, for this setup up to 100 data points are available to minimise the objective function for one single position along the radargram.

Air wave travel times are required since, in most GPR surveys, the absolute start-of-trace signal (time zero) is not available. Instead, the travel time of the air wave, with its known velocity, is used as a reference. Since, with the applied system, amplitudes of air wave signals measured with long antenna separations are often very low, picking of the accurate air wave travel time is difficult or even impossible. To overcome this difficulty we used the air wave adaptation procedure of Gerhards et al. (2008) which is based on the multi-channel evaluation. It slightly shifts the air wave travel times from the initial estimates of each channel such that for different sets of transmitter–receiver combinations consistent values for relative dielectric permittivity and reflector depth are obtained. In order to confine the inverse adaptation of air wave travel times to a reasonable range, the air wave travel times of the channels with 0.19 m antenna separation (T2–R2 and T3–R3), which were well identifiable in the radargrams, were first picked and then fixed to a constant average travel time which was calculated for both channels individually. Subsequently, air wave travel times of all other channels

were adjusted by using the air wave adaptation algorithm. This procedure was done for each of the eight transects individually in order to account for a possible drift of the antenna electronics. For data evaluation, we use constant air wave travel times for each individual radargram. The application of the air wave adaptation method may cause a certain bias on the estimated absolute relative dielectric permittivities and the related reflector depths and average soil moisture contents. However, relative changes in these parameters within the data set will still be recognisable after this correction (Gerhards et al., 2008).

The average volumetric water content θ [–] of the unfrozen active layer was calculated from the estimated relative dielectric permittivities according to Roth et al. (1990) for each position along the radargram by using the CRIM (Complex Refractive Index Method) formula:

$$\theta = \frac{\sqrt{\varepsilon_c} - \sqrt{\varepsilon_s} - \phi(1 - \sqrt{\varepsilon_s})}{\sqrt{\varepsilon_w} - 1}, \quad (3)$$

where ε_c [–] is the composite dielectric permittivity of the soil, ε_s [–], ε_w [–], ε_a [–] are the dielectric permittivities of the solid matrix, water and air, respectively, and ϕ [–] is porosity. The dielectric permittivity of water was set to a constant value of 86.1 corresponding to a soil temperature of 5°C (Kaatze, 1998). For the dielectric permittivity of the solid matrix we assumed a constant value of $\varepsilon_s = 5$, and set the porosity to an estimated fixed value of $\phi = 0.4$.

For plotting of the radargrams we considered topography by shifting each trace vertically by 0.1 ns per meter height difference. For spatial visualisation of the data acquired from all eight transects, contour plots of surface and reflector topography, depth of the reflector below the ground surface and avarage volumetric soil moisture content were generated by a simple bi-linear interpolation of the values measured along the different transects.

4 Results and discussion

4.1 Example transect

Example radargrams for all eight channels derived from a multi-channel measurement along one selected transect are shown in Fig. 4. The data were recorded along a measurement line upslope of the roadside ditch partly traversing bare soil and partly the vegetated area. In the middle of the transect a non-vegetated section within the vegetated part of the site was crossed. All radargrams show one dominant reflection from the frost table which is well detectable on each channel. Below the vegetated area, at long antenna separations, the reflection becomes weak or even disappears. We presume that this effect occurs due to the rough ground surface an the longer travel path for larger antenna separations. The first affects the orientation of the different antennas relative to each other. This, in turn, influences the orientation of the radiation pattern. Therefore, setups can occur where only little energy is emitted in the direction of the signal measured by the receiver. Furthermore, the longer travel path for large antenna separations lead to stronger decay of the energy due to dissipation and geometrical spreading. In addition, the rough surface of the vegetated patch leads to a weaker antenna-ground-coupling which results in a weaker signal.

In general, the shape of the reflector indicated by its two-way travel time follows the surface topography. Although, travel times are slightly longer below the bare soil sections than below the vegetated sections. At a first glance, this indicates either a deeper frost table and/or a higher soil moisture content in this area compared to the vegetated patch.

Figure 5 shows the topographically corrected, estimated reflector depth, relative dielectric permittivity and average volumetric soil moisture content of the unfrozen active layer as derived from the multi-channel analysis for the example survey line displayed in Fig. 4. All values are shown with both full spatial resolution and smoothed with a linearly weighted running mean filter calculated with 2 m support. In addition and for comparison, the reflector depth was calculated for a constant dielectric permittivity of

ε_c=15 as estimated from the multi-channel inversion for most sections of the bare soil areas. It corresponds to a constant signal velocity of 0.08 m ns^{-1}.

The topography of the reflector below the ground surface estimated from the multi-channel inversion appears rather rough. Besides a real rough frost table surface this may also result from local variations in dielectric permittivity of the unfrozen active layer or small variations in the effective antenna separation when the single antennas move across the hilly vegetated area and thereby slightly change their orientation relative to each other. The latter effect is not considered during the data processing. Hence, in the following, we will concentrate on the discussion of major variations in reflector depth and average soil moisture content which are large compared to the – potentially systematic – noise.

As it was already observed from the travel times displayed in the radargrams (Fig. 4), the inverted frost table depth (red and blue lines) generally follows surface topography but differences between bare soil and vegetated sections along the transect appear not as obvious as indicated by the signal travel times. In contrast, calculations with a constant dielectric permittivity of ε_c=15 (Fig. 5, green line) lead to an up to 0.5 m shallower frost table beneath the vegetated patch compared to the estimates with variable dielectric permittivity.

The relative dielectric permittivity and the related average volumetric soil moisture content inferred from the multi-channel analysis show strong variations along the transect (Fig. 5). On the first approximately 10 m of the radargram, below a bare soil section, moisture contents are rather high and then decrease sharply when entering the vegetated area. Below the section of the profile where vegetation and accumulations of fine sand at the soil surface are missing (~30...40 m), relative dielectric permittivity, hence average soil moisture content, rises abruptly and drops again as the following vegetated patch is crossed. Within the adjacent bare soil section, average volumetric soil moisture content and relative dielectric permittivity are again high and remain at these values for the final section of the radargram. The analysis clearly shows, that differences in observed travel times (Fig. 4) are not exclusively related to changes in

reflector depth. They strongly depend on lateral variations in average soil moisture content which changes significantly while crossing the bare and vegetated units along the transect. Short travel times beneath the vegetated area are caused by a low volumetric soil moisture content while longer travel times in the bare soil section are strongly related to a higher soil moisture content in this area. Assuming one single propagation velocity for the GPR signal for the complete measurement line (Fig. 5, green line) leads to severe deviations of the estimated reflector depth from the real situation. Without showing the results, we comment that similar observations with high relative dielectric permittivities, hence average volumetric soil moisture contents below the bare soil areas and low values below the vegetated area were made for the other radargrams crossing the vegetated area.

4.2 Spatial data

Contour plots of surface and reflector topography, thaw depth below ground surface, and average volumetric soil moisture content of the unfrozen active layer are shown in Fig. 6. The large-scale topography of the reflecting frost table generally follows the surface topography. Neglecting the slope and looking only at the thickness of the thawed active layer, one can clearly observe a shallower frost table beneath the vegetated area even if variations in dielectric permittivity along the transect are considered. In this area, where the ground surface is also higher than the surrounding region, the frost table builds a shallow mound below the vegetation. In addition, a shallow frost table was observed along the roadside ditch which results from its lower topographic height compared to the adjacent measurement lines which apparently is not able to "burn" into the frost table. This is possibly due to its higher water content from enhanced infiltration. Upslope of the road, in the bare soil sections surrounding the vegetated area, the depth of the frost table is about 0.3 m to 0.7 m deeper than underneath the vegetated patch. Similar to slightly shallower frost table depths were derived for the transect along the road and the two profiles downslope of the gravel road.

Measured average soil moisture contents are lowest underneath the vegetated patch

and rise beneath the directly surrounding bare soil area. With greater distance to the vegetated patch, average soil moisture contents decrease again in the upslope area of the bare soil sections. Highest average soil moisture contents were detected below the gravel road, the adjacent roadside ditch, and along the profiles measured in the valley bottom downslope of the road.

4.3 Discussion of the observed frost table depths and average soil moisture contents

The observed late-summer patterns of thaw depth and soil moisture content are the result of various short and long-term processes that interact during the thawing season. Since our data only represent one point in time and additional continuous observations like meteorological variables, soil moisture conditions or snow cover are not available, we can only hypothesise about the processes that led to the observed thaw patterns.

For the following discussion the site is divided into three major units: (i) the bare soil area upslope of the Xinjang-Tibet Highway which is characterised by a relatively deep frost table and low to intermediate average soil moisture contents, (ii) the vegetated, fine sand area with shallowest thaw depths and low soil moisture contents, and (iii) the gravel road and its downslope area with a high volumetric soil moisture content and intermediate thaw depths.

From our observations, differences in the active layer thaw depth measured in the study area can primarily be related to variations in soil texture and the corresponding soil moisture content, vegetation cover and albedo which allow to interpret the differences in energy transfer between soil and atmosphere. In addition, we can make some hypotheses about the thawing process between its initiation in early summer and the observed late-summer situation.

In early summer, runoff primarily occurs as surface runoff on the almost completely frozen ground surface. Surface topography diverts the flow and guides it along the existing channels. Surface runoff will pass around the elevated vegetation patch and discharge into the valley bottom along the riverbed that extends parallel to the road.

Surface albedo is lower in the wet areas than in their surroundings which allows a larger ground heat flux compared to the dry regions. With the infiltrating, already warm surface water, the thawing front proceeds faster through the coarse textured material. Later, runoff primarily occurs as groundwater flow which can again be expected to be concentrated primarily within the coarse textured materials of the site. However, a groundwater table will also develop above the ice table in the fine textured material, even if groundwater flow can be expected to mainly occur in the coarse textured sediments covering the site. The high density of the roadbed together with its low average pore size and correspondingly low hydraulic conductivity will generally cause a high moisture content within this unit. These properties may also induce ponding of discharging groundwater from the upslope area and favour the settlement of grass in the fine textured areas close to the road bed due to their higher water retention capacity and initially high groundwater levels here. The measured intermediate thaw depth beneath the roadbed and the downslope area may in part be a result of thermal erosion of infiltrating water within this main discharge area of the catchment.

Since the site is located in a desert environment, precipitation is very small. Hence, during summer, after infiltration from runoff has ceased, the unsaturated, coarse grained sediments in the bare soil sections can be expected to have a lower water content than the fine textured areas due to their lower water retention capacity. This would lead to a higher ground heat flux and a deeper active layer thaw depth in the bare soil section compared to the fine textured patch as it also has been observed during the survey. The measured high soil moisture content in the bare soil region appears to disagree with this interpretation. One has to realize, however, that the measured *average* soil moisture content originates from the shallow groundwater body on top of the frost table on the one hand and of the water in the soil matrix which is held by capillary forces. The GPR method applied here is not able to resolve the vertical water content distribution. Since the ice table below the vegetation is obviously more shallow, the same is true for the groundwater. Hence, the *average* soil moisture content is lower. We interpret the comparably low average soil moisture contents measured in

the bare soil areas farther away from the vegetated patch by the deeper frost table in this region. An equal thickness of the groundwater body here leads to a lower average soil moisture content as inferred from the GPR measurements.

Within the fine textured, vegetated area, the observed shallow thaw depth and low soil moisture content may result from a combination of a number of factors. In general, the grass cover is rather sparse, hence the shielding effect of the vegetation cover may be regarded to be rather negligible compared to the dense vegetation covers which are known for peat soils in other permafrost regions. With respect to the subsurface phenomena in the fine-textured area, in early summer, at still high groundwater levels, the higher water retention capacity of the fine-textured material will allow a higher capillary rise of water from the groundwater table in this area. This favours the availabiltity of water for evaporation which, again, has a cooling effect in this area. The observed precipitations of surface salt potentially increase the albedo compared to the surrounding bare soil regions which leads to a stronger reflection of solar radiation and therefore reduces the energy transfer into the soil. In addition, the increased availability of near-surface water within the fine textured area may have promoted the settlement of plants in this region. The sparse grass cover in combination with the sand accumulations at the soil surface increases surface roughness in this area. This may induce more turbulent fluxes which aid in removing sensible and latent heat from the soil surface, thus enhancing the cooling of the subsurface. We expect that the sum of these processes lead to a lower energy transfer into the soil of the vegetated patch favouring a shallower thaw depth within this area. With respect to soil moisture content we presume that the measured low average water content primarily originates from water that is held by capillary forces and that groundwater is almost missing here. The absolute elevation of the frost table within the vegetated area is higher than in the surrounding bare soil regions. Consequently, we expect groundwater discharging from upslope areas to flow around the patch and through the coarser grained sediments of the bare soil sections. The same is true for surface runoff, which indeed may be the starting point – in early summer – of this differentiation.

5 Summary and conclusions

Multi-channel ground-penetrating radar was applied at a continuous permafrost site on the Tibetan Plateau in order to investigate the influence of surface and soil textural properties on the late-summer thaw depth of the active layer. Even if conducted on a rather small example site with strongly varying surface and soil textural conditions, this investigation demonstrated the potential of multi-channel ground penetrating radar to efficiently map thaw depth and average soil moisture content of the active layer with high spatial resolution.

From our measurements, we found plausible hypotheses for the permafrost dynamics at this site. Surface and subsurface factors (topography, vegetation, albedo, soil texture and soil moisture content) strongly influence the shape of the frost table. This influence is far from trivial, however, since surface and subsurface factors and processes interact in a complicated manner: Instead of a naively expected high amount of water in the fine textured soil the amount was lower than in the surrounding coarse-textured soil due to complicated interactions:

- Surface topography diverts early-summer surface flows around the vegetated patch and decreases the albedo of the wet surfaces.
- With the already warm surface water, lower albedo and higher ground heat flux, the thawing front proceeds faster through the coarse textured material, leading to the observed deep thaw depth.
- A higher evaporation flux in the fine-textured material reduces the ground heat flux and soil moisture content. The cooling effect is enhanced by removal of heat due to turbulent fluxes on top of the rough surface, a higher albedo caused by salt precipitations, and shielding of the ground surface by the vegetation.
- At the end of the thawing season, subsurface flow continues to be diverted around the vegetation patch due to the evolving hump in the frost table.

The multi-channel GPR technique efficiently covers the intermediate scales between traditional point measurements and space-based remote sensing. In this way, it provides spatial information about meso-scale heterogeneity of active layer parameters that is hard to obtain otherwise. This opens a way for more detailed investigations of ecosystem dynamics in permafrost environments. In addition, the technique yields spatial information of subsurface parameters which can be used as ground-truth data to calibrate and interpret remote sensing data and results from permafrost models.

Acknowledgements. We thank our collegues from the Cold and Arid Regions Environmental and Engineering Research Institute (CAREERI), Lanzhou, especially Huijun Jin, for logistical support during field work. We are greatful to Philip Schiwek and Xicai Pan for their assistance in the year 2006 GPR measurements. This investigation was funded in part by the Deutsche Forschungsgemeinschaft (DFG): project RO 1080/10-1. The travel expenses for field work were funded by the Outstanding Youth Foundation Project, the National Natural Science Foundation of China (Grant No. 40625004), Chinese Academy of Sciences 100 Talents Program (Grant No. CAREERI-O481811).

References

Annan, A. P. and Davis, J. L.: Impulse radar sounding in permafrost, Radio Sci., 4, 383–394, 1976. 922

Arcone, S. A., Lawson D. E., Delaney, A. J., and Strasser, J. C.: Ground-penetrating radar reflection profiling of groundwater and bedrock in an area of discontinuous permafrost, Geophysics, 63, 1573–1584, 1998. 922, 923

Bradford, J. H., McNamara, J. P., Bowden, W., and Gooseff, M. N.: Measuring thaw depth beneath peat-lined arctic streams using ground-penetrating radar, Hydrol. Proc., 19, 2689–2699, 2005. 922

Bradford, J. H.: Measuring water content heterogeneity using multifold GPR with reflection tomography, Vadose Zone J., 7, 184–193, 2008. 923

Brosten, T. R., Bradford, J. H., McNamara, J. P., Zarnetske, J. P., Gooseff, M. N., and Bowden, W.: Profiles of temporal thaw depths beneath two arctic stream types using ground-penetrating radar, Permafrost Periglac. Proc., 17, 341–355, 2006. 922

Brosten, T. R., Bradford, J. H., McNamara, J. P., Gooseff, M. N., Zarnetske, J. P., Bowden, W. B., and Johnston, M. E.: Estimating 3D variation in active-layer thickness beneath arctic streams using ground-penetrating radar, J. Hydrol., 373, 479–486, 2009. 922

Brown. J., Hinkel, K. M., and Nelson, F. E.: The Circumpolar Active Layer Monitoring (CALM) Program: Research designs and initial results, Polar Geogr., 24, 165–258, 2000. 921

Cheng, G. and Wu, T.: Responses of permafrost to climate change and their environmental significance, Qinghai-Tibet Plateau. J. Geophys. Res., 112, F02S03, doi:10.1029/2006JF000631, 2007. 920

Davis, J. L. and Annan, A. P.: Ground-penetrating radar for high-resolution mapping of soil and rock stratigraphy, Geophys. Prospect., 37, 531–551, 1989. 922

Duguay, C. R., Zhang, T., Leverington, D. W., and Romanovsky, V. E.: Satellite remote sensing of permafrost and seasonally frozen ground. In: Duguay, C.R. and Pietroniro, A.: Remote sensing in northern hydrology. Measuring environmental change. AGU Geophysical Monograph 163, 91–118, 2005. 921, 922

Gasse, F., Arnold, M., Fontes, J. C., Fort, M., Gibert, E., Huc, A., Li Bingyan, Li Yuanfang, Liu Qing, Mélières, F., Van Campo, E., Wang Fubao, and Zhang Qingsong: A 13.000-year climate record from western Tibet, Nature, 353, 742–745, 1991. 924

Gerhards, H., Wollschläger, U., Yu, Q., Schiwek, P., Pan, X., and Roth, K.: Continuous and simultaneous measurement of reflector depth and average soil-water content with multichannel ground penetrating radar, Geophysics, 73, J15–J23, doi:10.1190/1.2943669, 2008. 923, 924, 927, 928, 929

Greaves, R. J., Lesmes, D. P., Lee, J. M., and Toksöz: Velocity variations and water content estimated from multi-offset ground-penetrating radar, Geophysics, 61, 683–695, 1996. 923

Hinkel, K. M., Doolittle, J. A., Bockheim, J. G., Nelson, F. E., Paetzold, R., Kimble, J. M., and Travis, R.: Detection of subsurface permafrost features with ground-penetrating radar, Barrow, Alaska, Permafrost Periglac. Process., 12, 179–190, 2001. 922

Hinkel, K. M. and Nelson, F. E.: Spatial and temporal patterns of active layer thickness at Circumpolar Active Layer Monitoring (CALM) sites in northern Alaska, 1995–2000, J. Geophys. Res., 108, D2, 8168, doi:10.1029/2001JD000927, 2003. 921

Hinzman, L. D., Bettez, N. D., Bolton, W. R., et al.: Evidence and implications of recent climate change in northern Alaska and other arctic regions, Clim. Change, 72, 251–298, 2005. 921

Jin, H., Chang, X. L., and Wang, S. L.: Evolution of permafrost on the Qinghai-Xizang (Tibet) Plateau since the end of the late Pleistocene, J. Geophys. Res., 112, F02S09,

doi:10.1029/2006JF000521, 2007. 924
Kaatze, U.: Complex permittivity of water as a function of frequency and temperature, J. Chem. Eng. Data, 34, 371–374, 1998. 929
Kane, D. L., Hinzman, L. D., and Zarling, J. P.: Thermal response of the active layer to climatic warming in a permafrost environment, Cold Reg. Sci. Technol., 19, 111–122, 1998. 921
Lemke, P., Ren, J., Alley, R. B., Allison, I., Carrasco, J., Flato, G., Fujii, Y., Kaser, G., Mote, P., Thomas, R. H., and Zhang, T.: Observations: Changes in snow, ice and frozen ground, in: Climate Change 2007: The Physical Science Basis. Contribution of Working Group I to the Fourth Assessment Report of the Intergovernmental Panel on Climate Change, edited by: Solomon, S., Qin, D., Manning, M., Chen, Z., Marquis, M., Averyt, K. B., Tignor, M., and Miller, H. L., Cambridge University Press, Cambridge, UK and New York, NY, USA, 2007. 921
Liu, X. and Chen, B.: Climatic warming in the Tibetan Plateau during recent decades, Int. J. Climatol., 20, 1729–1742, 2000. 920, 921
Lunt, I. A., Hubbard, S. S., and Rubin, Y.: Soil moisture content estimation using ground-penetrating radar reflection data, J. Hydrol., 307, 254–269, 2005. 923
Moorman, B. J. , Robinson, S. D., and Burgess, M. M.: Imaging periglacial conditions with ground-penetrating radar, Permafrost Periglac. Process., 14, 319–329, 2003. 922
Munroe, J. S., Doolittle, J. A., Kanevskiy, M. Z., Hinkel, K. M., Nelson, F. E., Jones, B. M., Shur, Y., and Kimble, J. M.: Application of ground-penetrating radar imagery for three-dimensional visualization of near-surface structures in ice-rich permafrost, Barrow, Alaska, Permafrost Periglac. Proc., 18, 309–321, 2007. 922
Neal, A.: Ground-penetrating radar and its use in sedimentology: principles, problems and progress, Earth-Sci. Rev., 66, 261–330, 2004. 923
Nelson, F. E., Anisimov, O. E., and Shiklomanov, N. I.: Subsidence risk from thawing permafrost, Nature, 410, 889, 2001. 921
Roth, K., Schulin, R., Flühler, H., and Attinger, W.: Calibration of time domain reflectometry for water content measurement using a composite dielectric approach, Water Resour. Res., 26, 2267–2273, 1990. 929
Schwamborn, G., Wagner, D., and Hubberten, H.-W.: The use of GPR to detect active layers in young periglacial terrain of Livingston Island, Maritime Antarctica, Near Surf. Geophys., 331–336, 2008. 922, 923
van Everdingen, R. ed.: Multi-language glossary of permafrost and related ground-ice terms.

National Snow and Ice Data Center/World Data Center for Glaciology, Boulder, CO, 1998, revised May 2005, http://nsidc.org/fgdc/glossary/. 921

Walker, D. A., Jia, G. J., Epstein, H. E., Raynolds, M. K., Chapin III, F. S., Copass, C., Hinzman, L. D., Knudson, J. A., Maier, H. A., Michaelson, G. J., Nelson, F., Ping, C. L., Romanovsky, V. E., and Shiklomanov, N.: Vegetaion-soil-thaw-depth relationships along a low-arctic bioclimate gradient, Alaska: Synthesis of information from the ATLAS studies, Permafrost Periglac. Proc., 14, 103–123, 2003. 921

Wollschläger, U. and Roth, K.: Estimation of temporal changes of volumetric soil water content from ground-penetrating radar reflections, Subsur. Sens. Technol. Appl., 6, 207–218. 923

Wright, N., Hayashi, M., and Quinton, W. L.: Spatial and temporal variations in active layer thawing and their implication on runoff generation in peat-covered permafrost terrain, Water Resour. Res., 45, W05414, doi:10.1029/2008WR006880, 2009. 921

Yoshikawa, K., Leuschen, C., Ikeda, A., Harada, K., Gogineni, P., Hoekstra, P., Hinzman, L., Sawada, Y., and Matsuoka, N.: Comparison of geophysical investigations for detection of massive ground ice (pingo ice), J. Geophys. Res., 111, E0619, doi:10.1029/2005JE002573, 2006. 922

Zhang, T., Barry, R. G., and Armstrong, R. L.: Applications of satellite remote sensing techniques to frozen ground studies, Pol. Geogr., 28, 163–196, 2004. 922

Zhou, Y. and Guo, D.: Some features of permafrost in China, Proc. 4th Int. Conf. on Permafrost, 17–22 July 1983, Fairbanks, Alaska, Natl. Academy Press, Washington DC, USA, 1496–1501, 1983. 924

Zhou, Y., Guo, D., Qiu, G., and Cheng, G.: Ceocryology in China (in Chinese), Beijing: Science Press, 165–167, 2000. 924

Zhou, Z., Baoyin, Y., and Petit-Maire, N.: Paleoenvironments in China during the Last Glacial Maximum and the Holocene Optimum, Episodes, 21, 152–158, 1998. 924

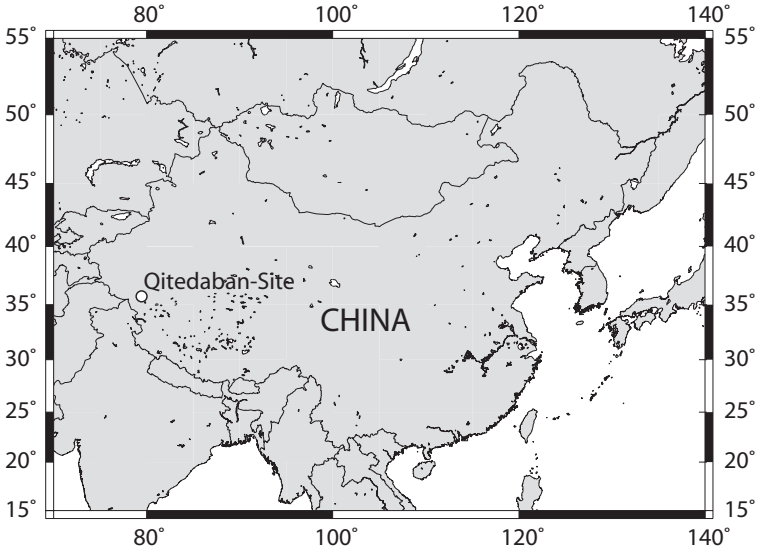

Fig. 1. Geographical position of the Qitedaban-Site (35° 45′ N, 79° 26′ E, 4950 m a.s.l.).

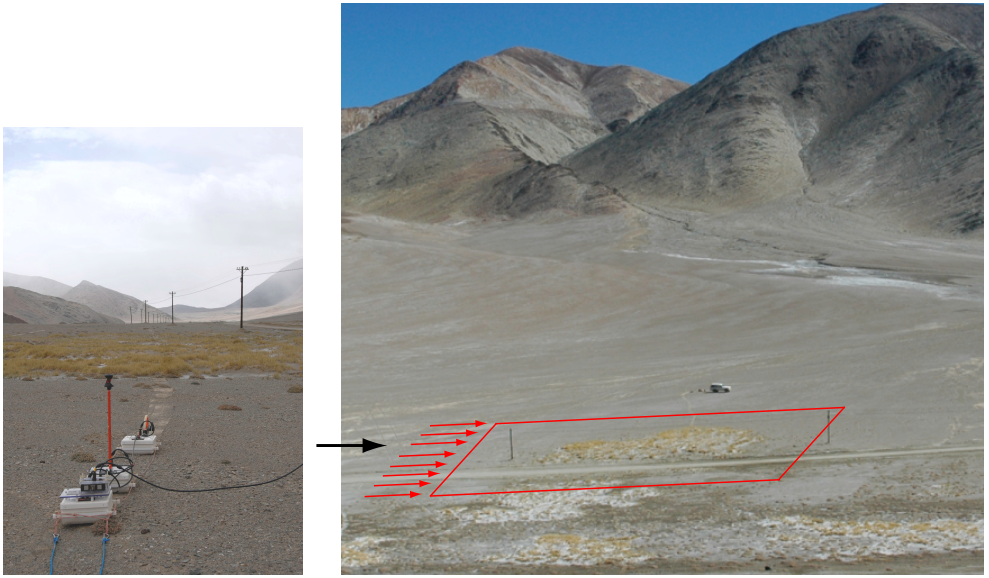

Fig. 2. Photographs of the study area: GPR measurements were acquired at the foot of an alluvial fan, partly across bare soil, a small vegetated area and the roadbed of the Xinjiang-Tibet Highway (red box; arrows indicate the direction of GPR lines as shown in Sect. 4). A detailed photograph of the vegetated area and the adjacent bare soil is provided on the left photograph, the black arrow indicates the location and viewing direction of the photograph at the left.

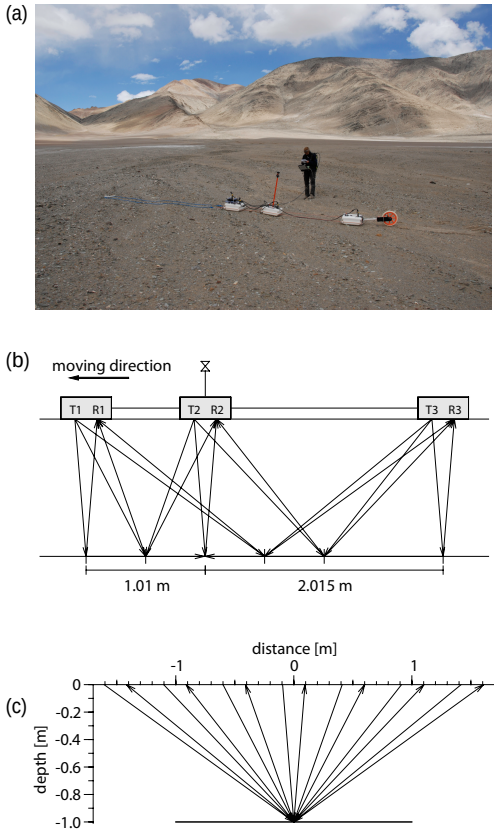

Fig. 3. (a) Photograph of an 8 channel setup. **(b)** Sketch of the 9 possible transmitter–receiver combinations. For analysis, radargrams are shifted to a common reflection point, here to the position where the reflector of the tachymeter is mounted on the middle antenna. **(c)** CMP pathways after lateral shift of radargrams.

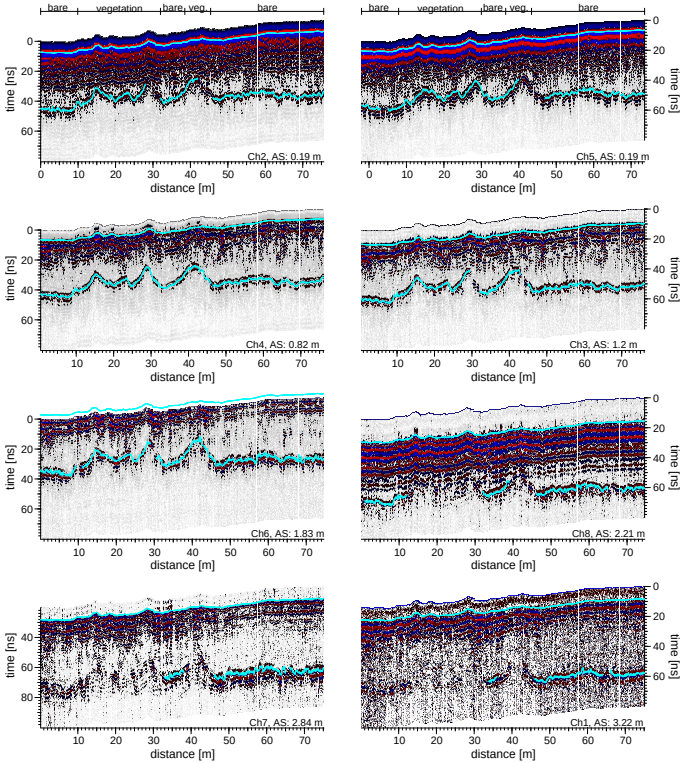

Fig. 4. Example radargrams from all 8 channels showing a measurement which traversed both, bare soil and the vegetated area. Vegetated and bare soil sections are indicated in the topmost radargrams. Air wave and ground wave travel times are drawn in light blue, antenna separations (AS) are given at the lower right of each radargram. Below the vegetated areas the reflection from the frost table is not clearly visible at long antenna separations.

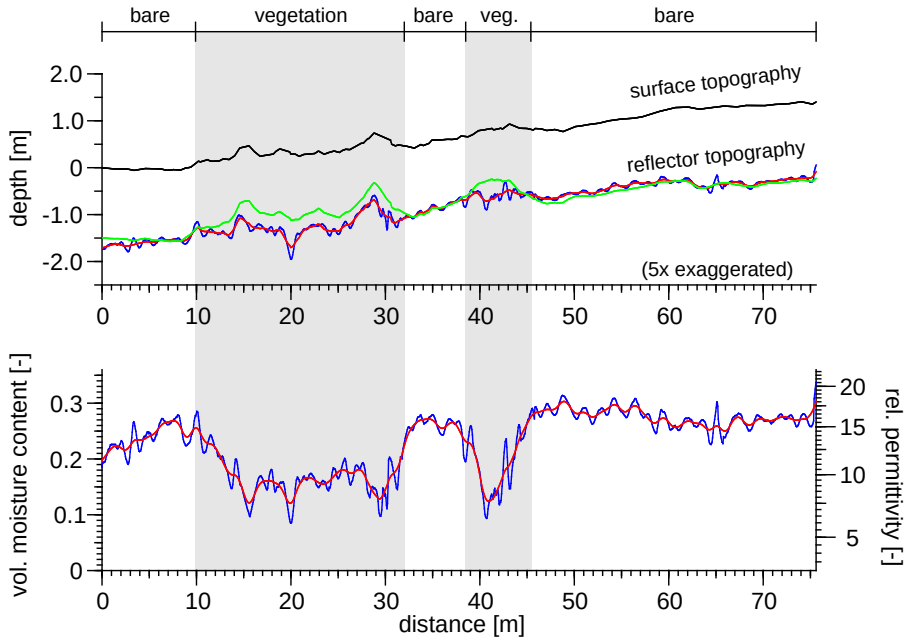

Fig. 5. Surface topography, reflector depth (top graph), average volumetric soil moisture content and relative dielectric permittivity (bottom graph) inferred for the example transect shown in Fig. 4; blue: raw data, red: data averaged using a linearly weighted running mean filter over a distance of 2 m, green: reflector depth calculated with a constant dielectric permittivity of ε_c=15.

TCD
3, 919–946, 2009

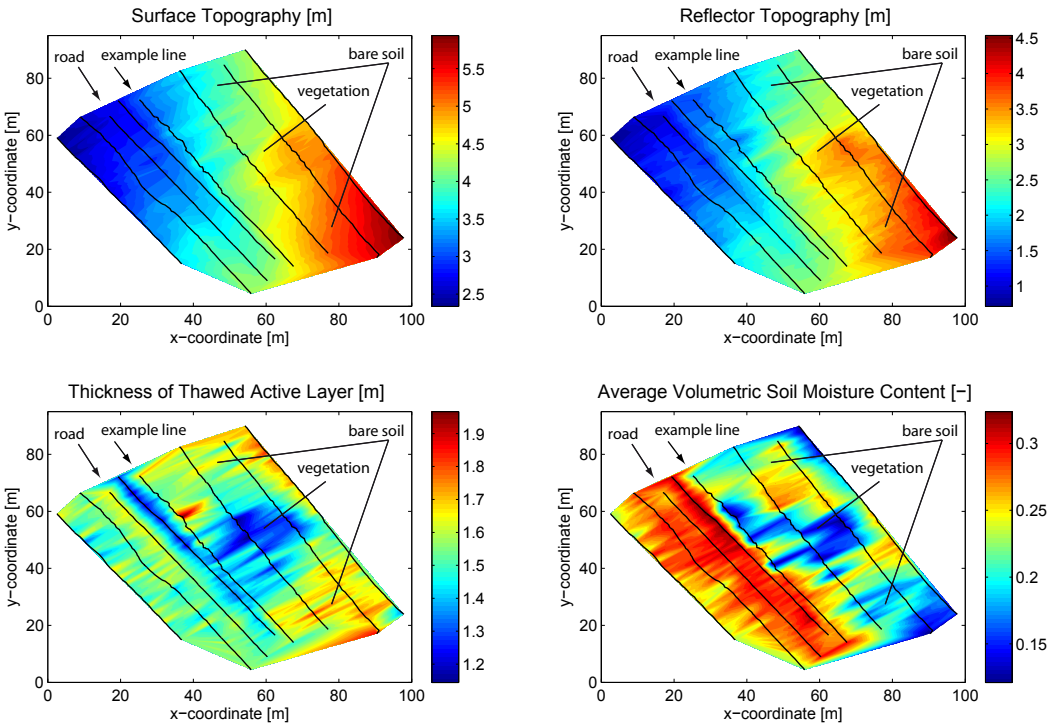

Fig. 6. Surface and reflector topography, thaw depth, and average soil moisture content calculated for the active layer within the measurement area. Black lines indicate positions of GPR profiles. For better orientation, the positions of the gravel road, vegetated and bare soil area, and the example line discussed in Figs. 4 and 5 are indicated separately.